arrangement of the positive and negative ions in each layer plane (quadrupole symmetry), such modulation of the polar order may not be observed. In fact, the N-LC film, possessing quadrupole symmetry in the ionic layers, was inactive at all for the SHG under the same experimental condition. On the basis of these preliminary results, therefore, we concluded that the SHG from the P-LC film may be governed by the customary electric dipole process rather than the electric quadrupole process.

[13] a) *Nonlinear Optical Properties of Organic Molecules and Crystals, Vol. 1* (Eds.: D. S. Chemla, J. Zyss), Academic Press, Orlando, FL, **1987**, pp. 63–72; b) H. Hsiung, Y. R. Shen, *Phys. Rev. A* **1986**, *34*, 4303.

[14] ANCHOR II V1L5, Fujitsu, Ltd., Kureha Chemical Industry, Co. Ltd., Tokyo, **1995**.

Global Chirality in Rigid Decametallic Ruthenium Dendrimers**

Mahn-Jong Kim, Frederick M. MacDonnell,* Mary E. Gimon-Kinsel, Thomas Du Bois, Niloofar Asgharian, and James C. Griener

One hallmark of dendrimer chemistry is the ability to construct nanometer-sized assemblies with discrete architectures and defined connectivity.[1] In many cases, however, the ability to control the primary structure does not translate into the ability to control the global structure with high spatial organization and fidelity. Conformational flexibility within the dendrimer often leads to compact "molten globule" tertiary structures despite the composition. The incorporation of rigid monomers and linkages has led to shape-persistent dendrimers with restricted conformations, however, some rotational motion prevents complete spatial control.[2] A related, but heretofore elusive, goal is the construction of dendrimers that exhibit a global chiral topology.[3] Efforts to impart such a "tertiary" structure have focused predominantly on the incorporation of chiral carbon centers (C_1 symmetric) into the "primary" structure of the dendrimer.[4] While interesting chirooptic effects are observed in several cases, none show adoption of a preferred global chiral structure.

In contrast, spatially well-defined nanoscopic molecules, such as helicates, rings, squares, and boxes, are readily assembled by using metal-directed self-assembly methods.[5] Many such structures exhibit macroscopic chirality and several have even been prepared in enantiopure form through the use of chiral ligands.[6] The self-assembly approach has one drawback, in that the high lability of the metal ions required for such facile assembly typically makes such structures equally susceptible to decomposition or reorganization under conditions far milder than observed for most dendrimers.

We describe herein the synthesis of chiral, conformationally rigid metallodendrimers, which rival organic dendrimers in robustness and self-assembled structures in spatial fidelity. The $[Ru(diimine)_3]^{2+}$ unit is our basic chiral synthon for supramolecular synthesis. This unit has enjoyed considerable attention as a building block for metallodendrimers largely because of its favorable room-temperature luminescence and redox properties, as well as its excellent chemical stability.[7] Until recently, however, the lack of stereospecific synthetic methods in the preparation of multimetallic assemblies has meant that such dendrimers are diastereomeric mixtures.[8] We have developed a stereospecific synthetic strategy for assembling such units into dendritic arrays and now demonstrate the power of this method to direct the tertiary structure of a nanosized molecule.

The homochiral decamer $\Lambda_6\Lambda_3\Lambda$-**Ru$_{10}$** was prepared in enantiopure form following the divergent synthetic route shown in Scheme 1. The notation used, $\Lambda_6\Lambda_3\Lambda$-**Ru$_{10}$**, gives first the stereochemistry of the outermost shell of ruthenium atoms, then the stereochemistry of the next outermost ruthenium sites, and then of the core atom. Central to this strategy is the use of substitutionally inert ruthenium trisdiimine complexes as chiral synthons which are connected by the condensation reaction between quinone and diamine functional groups at the periphery. The ruthenium tetramer $[\Lambda\text{-Ru}\{\Lambda\text{-(tpphz)Ru(phen)}_2\}_3]^{8+}$ (tpphz = tetrapyrido[3,2-*a*:2′,3′-*c*:3″,2″-*h*:2‴,3‴-*j*]phenazine) ($\Lambda_3\Lambda$-**Ru$_4$**) was prepared by this method[9] and can act as the core for further dendritic growth after oxidation of the terminal phenanthrolines to the quinone product $\Lambda_3\Lambda$-**Ru$_4$one** (Scheme 1). In this manner, the parent hydrocarbon acts as the protected form of the quinone and permits a controlled growth scheme. This reaction gives 67% yield of the desired quinone and proceeds with retention of stereochemistry, despite the harsh reaction conditions, as determined by circular dichromism (CD) and by analogy to a model study of this reaction on mononuclear chiral complexes.[10] Addition of excess Λ-$[Ru(phen)_2(phendiamine)]^{2+}$ produces the decamer in ≈20% yield after purification by alumina- and gel-packed column chromatography. The diastereomeric decamer $\Lambda_6\Delta_3\Lambda$-**Ru$_{10}$** was prepared in a similar manner from $\Delta_3\Lambda$-**Ru$_4$one** and Λ-$[Ru(phen)_2$-(phendiamine)$]^{2+}$. Both show excellent solubility in acetonitrile or dimethyl sulfoxide as the hexafluorophosphate salt, or in water as the chloride salt. These complexes are robust and show good stability even under harsh conditions (heat, concentrated acids and bases) and are stable to racemization in the absence of intense irradiation.[11]

[*] Prof. F. M. MacDonnell, M.-J. Kim, Dr. N. Asgharian
Department of Chemistry and Biochemistry
The University of Texas, Arlington, TX (USA)
Fax: (+1) 817-272-3808
E-mail: macdonn@uta.edu
Dr. M. E. Gimon-Kinsel
Sensar Corporation, Provo, UT (USA)
Prof. T. Du Bois
Department of Chemistry
University of North Carolina, Charlotte, NC (USA)
Dr. J. C. Griener
Department of Pediatrics
The University of Texas Southwestern Medical Center, Dallas, TX (USA)

[**] This work was supported by the Robert A. Welch Foundation. We thank Prof. Zoltan Schelly for assistance and discussions in obtaining the electric birefringence data, Prof. Kurt Mislow for helpful discussions on stereochemistry, and Prof. Barton Kaman for use of the mass spectrometry equipment. The authors would also like to thank the North Carolina Supercomputing Center for their partial support of the computational component of this work.

  0570-0833/00/3903-0615 $ 17.50+.50/0

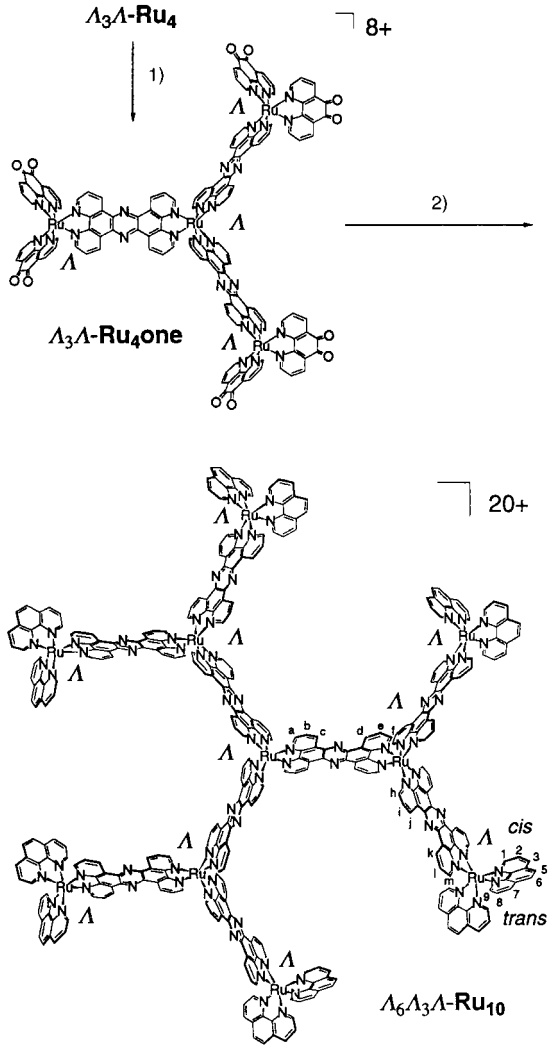

Scheme 1. Synthesis of the dendrimers. 1) H_2SO_4, HNO_3, NaBr, 100 °C; 2) 7 equiv Λ-[Ru(phen)$_2$(phendiamine)][PF_6]$_2$, MeCN/H_2O, reflux 15 h.

The decamers are composed of 448 non-hydrogen atoms (not including those of the anions), have a net 20+ charge, and have diameters estimated at >5 nm. The decameric structure of the cations, $[Ru_{10}C_{360}H_{204}N_{78}]^{20+}$, was confirmed using electrospray–ionization mass spectrometry (ESI-MS). For example, the spectrum of $\Lambda_6\Lambda_3\Lambda$-**Ru$_{10}$** as a 20[$PF_6$]$^-$ salt (Figure 1) clearly shows a dominant set of peaks corresponding to *m*/*z* of 915.3 ($\Lambda_6\Lambda_3\Lambda$-**Ru$_{10}$** − 9[$PF_6$])$^{9+}$, 809.4 ($\Lambda_6\Lambda_3\Lambda$-**Ru$_{10}$** − 10[$PF_6$])$^{10+}$, 722.7 ($\Lambda_6\Lambda_3\Lambda$-**Ru$_{10}$** − 11[$PF_6$])$^{11+}$, 650.6 ($\Lambda_6\Lambda_3\Lambda$-**Ru$_{10}$** − 12[$PF_6$])$^{12+}$, 589.4 ($\Lambda_6\Lambda_3\Lambda$-**Ru$_{10}$** − 13[$PF_6$])$^{13+}$, 537.1 ($\Lambda_6\Lambda_3\Lambda$-**Ru$_{10}$** − 14[$PF_6$])$^{14+}$, 491.7 ($\Lambda_6\Lambda_3\Lambda$-**Ru$_{10}$** − 15[$PF_6$])$^{15+}$, and 451.9 ($\Lambda_6\Lambda_3\Lambda$-**Ru$_{10}$** − 16[$PF_6$])$^{16+}$. A second set of much smaller peaks (marked with * in Figure 1) correspond to a defect structure that is missing one peripheral ruthenium complex ("**Ru$_9$**"). This impurity was not removed by chromatography but constitutes a minor component overall as determined by NMR spectroscopy (Figure 2). Previous studies of related metallodendrimers[12] have also shown that the PF_6^- ions can undergo extensive hydrolysis, which may be the source of the smaller baseline peaks.

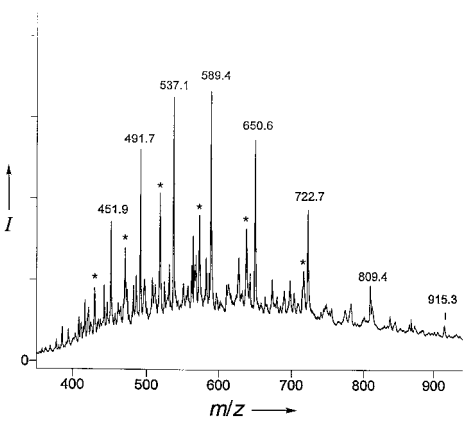

Figure 1. ESI-MS of ($\Lambda_6\Lambda_3\Lambda$-**Ru$_{10}$**)[$PF_6$]$_{20}$.

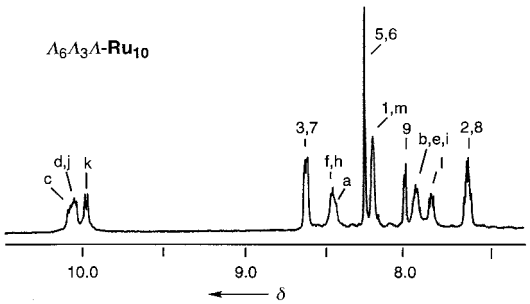

Figure 2. ^{1}H NMR of ($\Lambda_6\Lambda_3\Lambda$-**Ru$_{10}$**)[$PF_6$]$_{20}$ in [D_3]MeCN (500 MHz). Proton assignments shown in Scheme 1.

As shown in Figure 2, the D_3 symmetry of $\Lambda_6\Lambda_3\Lambda$-**Ru$_{10}$** is clearly evident in the simplicity of the ^{1}H NMR data. However, of the 20 peaks expected from symmetry considerations, only 12 somewhat broad peaks are clearly resolved. COSY data indicate the broadness is largely due to multiple overlapping peaks, which is not too surprising considering the similarity of the microenvironment about the core and intermediate ruthenium centers. Furthermore, we suspect the line broadening is partially an effect of the large size and colloidal behavior (see below) of these complexes in solution which slows molecular tumbling on the NMR time scale. The assignment of peaks in Figure 2 was made on the basis of COSY data, along with comparison to the previously described dimers and tetramers. The spectrum for $\Lambda_6\Lambda_3\Lambda$-**Ru$_{10}$** is nearly identical to that for $\Lambda_6\Lambda_3\Lambda$-**Ru$_{10}$**, differing significantly only in the location of H_a and H_c which are both shifted upfield by ≈0.05 ppm. The small residual peaks along the baseline at $\delta = 8.06$ and 8.33 show a small but detectable amount of the defect structure "**Ru$_9$**" is present.

Space-filling models of the two decamers (Figure 3) demonstrate the tertiary structure of the isomers. The stick-and-ball figures depict the spatial relationship and connectivity of ruthenium centers, and provide a simplified view of the global sterochemistry. Molecular modeling at the semiempirical level (PM3) was used to obtain the $[Ru(phen)_3]^{2+}$ core. This calculated structure was in excellent agreement with the crystallographic data for the same cation[13] and was used to construct models for the decameric structure (see Experimental Section). Due to the overall conformational rigidity, we believe the modeling provides a substantially accurate picture of the molecular topology.

  0570-0833/00/3903-0616 $ 17.50+.50/0 *Angew. Chem. Int. Ed.* **2000**, *39*, No. 3

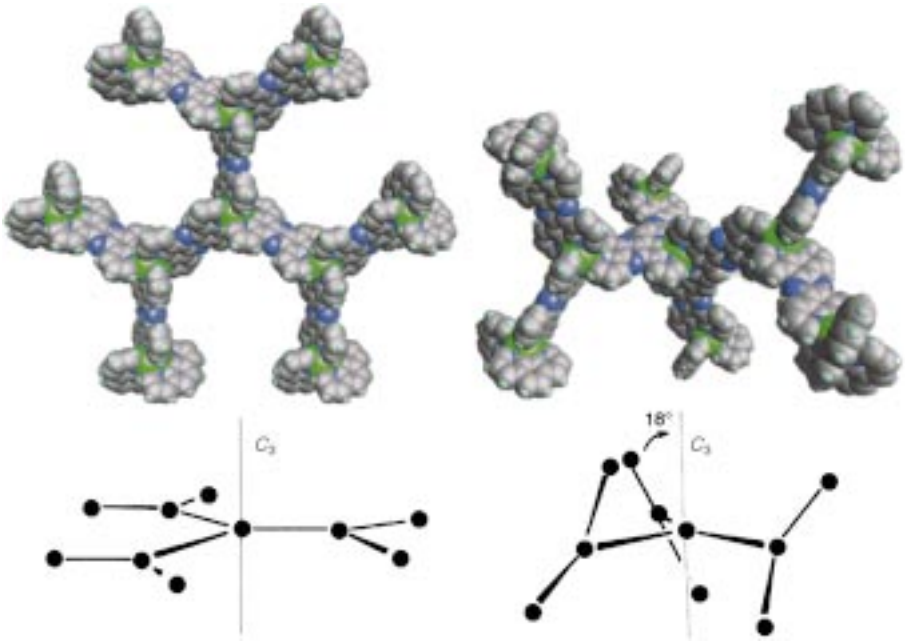

Figure 3. Space-filling models of (*T*)-($\Lambda_6\Delta_3\Lambda$-**Ru$_{10}$**) viewed down the molecular C_3 axis (left) and (*P*)-($\Lambda_6\Lambda_3\Lambda$-**Ru$_{10}$**) viewed perpendicular to the molecular C_3 axis (right) Green represents ruthenium and blue represents nitrogen atoms. Representative ball-and-stick drawings of the ruthenium atom connectivity and topology are shown below.

The two diastereomers differ only in the stereochemistry at three dendritic sites, however, this small change has a dramatic effect on the overall topology. When viewed from the central ruthenium core, each arm consists of a plane of four ruthenium centers. For $\Lambda_6\Lambda_3\Lambda$-**Ru$_{10}$**, the pitch angle of this plane relative to the molecular C_3 axis is $\approx 18^\circ$, resulting in a massive *right-handed* propeller structure. For $\Lambda_6\Delta_3\Lambda$-**Ru$_{10}$**, this pitch angle is 90° resulting in a flat disklike structure. The notation *P* (clockwise), *M* (counter-clockwise), and *T* (achiral) are introduced here as global stereochemical descriptors[14] to indicate the global helicity as depicted in Figure 3. Preparation of $\Delta_6\Delta_3\Delta$-**Ru$_{10}$** would give the *M* isomer. The macroscopic pitch angle is a direct consequence of the local 36° pitch angle relative to the C_3 axis found for the $[Ru(phen)_3]^{2+}$ synthons.[15] The core and adjacent stereocenter may combine constructively ($90^\circ - [36^\circ(\Lambda) + 36^\circ(\Lambda)] = 18^\circ$) to give the propeller structure or cancel ($90^\circ - [36^\circ(\Lambda) - 36^\circ(\Delta)] = 90^\circ$) to give the planar structure.

Surprisingly, despite these large differences in the global structure we do not observe any readily discernable features in the CD results that unambiguously can be attributed to either diastereomer. As observed in the diastereomeric dimers and tetramers,[13] the magnitude of the CD signal in the metal-to-ligand charge-transfer region (MLCT, 420–480 nm) is approximately proportional to the number of individual metal chromophores in enantiomeric excess (*ee*) within each structure. For the homochiral (*P*)-($\Lambda_6\Lambda_3\Lambda$-**Ru$_{10}$**) an intense molar CD of +178 (477 nm, MeCN) is observed, which is roughly a 10-fold increase over Λ-$[Ru(phen)_3]^{2+}$ (+21, 471 nm, MeCN). Complex (*T*)-($\Lambda_6\Delta_3\Lambda$-**Ru$_{10}$**) gives a molar CD of +76 at 464 nm corresponding to approximately four Λ-$[Ru(phen)_3]^{2+}$ chromophores in enantiomeric excess. The lack of CD features related to the global chirality in (*P*)-($\Lambda_6\Lambda_3\Lambda$-**Ru$_{10}$**) can be attributed to weak electronic coupling between chromophores.

Significantly, the differing topologies for (*T*)-($\Lambda_6\Delta_3\Lambda$-**Ru$_{10}$**) and (*P*)-($\Lambda_6\Lambda_3\Lambda$-**Ru$_{10}$**) do affect the colloidal properties as measured by electric birefringence. Campagna and coworkers have shown that related metallodendrimers are colloidal in dilute acetonitrile.[16] Dynamic light scattering experiments show that both (*T*)-($\Lambda_6\Delta_3\Lambda$-**Ru$_{10}$**) and (*P*)-($\Lambda_6\Lambda_3\Lambda$-**Ru$_{10}$**) exhibit polydisperse aggregation phenomena in acetonitrile (as PF_6^- salt) and water (as Cl^- salt). While no distinction between diastereomers could be observed in the light scattering experiment, both the amplitude and relaxation time for the forward and backwards birefringence signals (Figure 4) clearly show a distinct difference for the two colloids. For the *T* isomer (Figure 4b), the amplitude of the birefringence is small and the corresponding decay signal is fast (in the microsecond range). On the other hand, for the *P* isomer (Figure 4a) the amplitude of the birefringence is much larger and the decay far slower (in the millisecond range) and anomalous (full data is not shown). To confirm that this result is a consequence of differing topology and not simply the diastereotopic nature of the complexes, $\Lambda_3\Delta$-**Ru$_4$** and $\Lambda_3\Lambda$-**Ru$_4$** were examined. These two diastereomers have globally similar molecular topologies and also form polydisperse colloids in aqueous solution. In this control experiment, the birefringence signals were indistinguishable (both samples 0.22 mM as Cl^- salt in water). It is apparent that under the influence of an electric field, the isotropic chiral solution of (*P*)-($\Lambda_6\Lambda_3\Lambda$-**Ru$_{10}$**) becomes optically anisotropic, which is likely due to structural distortion/orientation of the aggregates in the direction of the field, *E*,

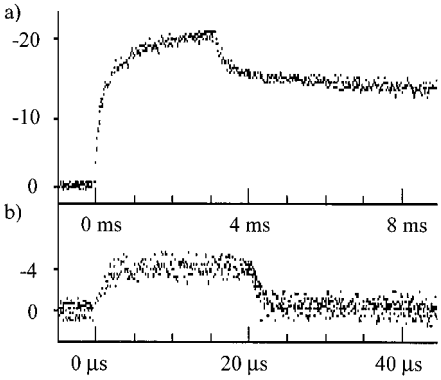

Figure 4. Plot of the electric field induced birefringence signals ($E = 4.8\ kV\,cm^{-1}$) of a) (*P*)-($\Lambda_6\Lambda_3\Lambda$-**Ru$_{10}$**) at 77 µM as Cl^- salt in water, with pulse length = 3 ms and b) (*T*)-($\Lambda_6\Delta_3\Lambda$-**Ru$_{10}$**) at 74 µM as Cl^- salt in water, with pulse length = 20 µs. The ordinate is proportional to the transmitted light intensity.

  0570-0833/00/3903-0617 $ 17.50+.50/0

whereas the rapid evolution of the birefringence for (*T*)-($\Lambda_6\Delta_3\Lambda$-**Ru$_{10}$**) can be attributed to electronic polarization. These dramatic results show the influence of tertiary structure on the colloidal and macroscopic properties of such systems. Full details of the dynamics of the physical events involved will be discussed in a forthcoming paper.

We believe our method for making enantiomerically pure and rigid metallodendrimers opens a unique passage into the realm of nanochemistry with the ability to synthesize robust, enantiopure, nanoscopic assemblies with precisely tailored structures. These shape-specific metallodendrimers can be compared with many proteins in that they exhibit specific tertiary structures as a consequence of their primary sequence (local stereochemistry, e. g. Λ-Λ-Λ versus Λ-Δ-Λ) and secondary structure (every four adjacent Ru atoms constitute a plane). Ultimately, we aim to use such structures as nanoscopic platforms from which larger nanoscopic or mesoscopic arrays may be constructed.

Experimental Section

The tetramers $\Lambda_3\Lambda$-**Ru$_4$**$[PF_6]_8$ and $\Delta_3\Lambda$-**Ru$_4$**$[PF_6]_8$ were synthesized according to literature procedures.[9]

The isomers of **Ru$_4$one**$[PF_6]_8$ were prepared by slow addition of the appropriate isomer of **Ru$_4$**$[PF_6]_8$ (0.1 g, 0.03 mmol) to concentrated H_2SO_4 (3 mL) chilled to 0 °C in an ice water bath. NaBr (0.125 g) and HNO_3 (2.5 mL) were added to the resulting solution, which was heated to 100 °C for 20 min, cooled to room temperature and then poured into chilled water (50 mL, 0 °C) containing $NaClO_4$ (5 g). After the mixture was allowed to stand for 12 h at 0 °C the precipitate was filtered, washed with water (3 mL) then slurried with Dowex 21 K anion exchange resin (Cl^- form, 10 g) in water (30 mL) for 30 min which slowly redissolved the product. The resin solution was filtered and addition of excess NH_4PF_6 to the supernatant produced an immediate precipitate which was filtered, washed with water (3 mL), and then extracted with MeCN (10 mL). The MeCN extract was treated with excess water to give a dark brown precipitate which was filtered, washed, and dried in the vacuum oven at 60 °C. Typical yield 0.063 g (60 %). Elemental analysis (%): $C_{144}H_{72}N_{30}F_{48}P_8Ru_4 \cdot 4H_2O$ calcd: C 42.70, H 1.99, N 10.37; found: C 42.79, H 1.79, N 10.62; ^{1}H NMR (500 MHz, [D$_3$]MeCN, 25 °C, TMS): $\delta = 10.05$ (d, $J = 10.0$ Hz, 6H), 10.03 (d, $J = 9.1$ Hz, 6H), 8.63 (d, $J = 7.8$ Hz, 6H), 8.53 (d, $J = 7.6$ Hz, 6H), 8.48 (d, $J = 4.7$ Hz, 6H), 8.44 (d, $J = 4.9$ Hz, 6H), 8.24 (d, $J = 4.9$ Hz, 6H), 8.07 (dd, $J_1 = 7.1$ Hz, $J_2 = 5.8$ Hz, 6H), 8.02 (d, $J = 5.1$ Hz, 6H), 7.98 (dd, $J_1 = 7.3$ Hz, $J_2 = 5.7$ Hz, 6H), 7.74 (dd, $J_1 = 7.4$ Hz, $J_2 = 6.1$ Hz, 6H), 7.53 (m, 6H); ESI MS: *m*/*z*: 1182 (**Ru$_4$one**-3$[PF_6]]^{3+}$, 850 (**Ru$_4$one**-4$[PF_6])^{4+}$, 651 (**Ru$_4$one**-5$[PF_6])^{5+}$, 519 (**Ru$_4$one**-6$[PF_6])^{6+}$, 424 (**Ru$_4$one**-7$[PF_6])^{7+}$; IR (KBr): $\tilde{\nu} = 1699$ cm^{-1} (C=O stretch).

$[\Lambda_6\Lambda_3\Lambda$-**Ru$_{10}$**$][PF_6]_{20}$ and $[\Lambda_6\Delta_3\Lambda$-**Ru$_{10}$**$][PF_6]_{20}$ were prepared similarly by addition of Λ-[Ru(phen)$_2$(phendiamine)]$[PF_6]_2$[17] (90 mg, 0.094 mmol, 7.2 equiv) to a solution of $\Delta_3\Lambda$-**Ru$_4$one**$[PF_6]_8$ or $\Delta_3\Lambda$-**Ru$_4$one**$[PF_6]_8$ (50 mg, 0.013 mmol), as appropriate, dissolved in MeCN/H_2O (2/1), and refluxing under N_2 for 15 h. After the mixture was allowed to cool, the product was precipitated by addition of NH_4PF_6 (30 mg) dissolved in water (5 mL) and removal of most of the MeCN by evaporation under vacuum. The reddish brown precipitate was purfied by column chromotography packed with neutral Al_2O_3 using 1 % NH_4PF_6 in MeCN (*m*/*v*) as eluent. The first band collected was then passed through a second column packed with lipophilic sephadex (LH-20) using MeCN/THF (1/1) as eluent. Typical yield 25 mg (21 %). Elemental analysis: $C_{360}H_{204}N_{78}F_{120}P_{20}Ru_{10}$ calcd: C 45.36, H 2.16, N 11.46; found: C 45.85, H 2.43, N 11.10.

$[\Lambda_6\Delta_3\Lambda$-**Ru$_{10}$**$][PF_6]_{20}$: ^{1}H NMR (500 MHz, [D$_3$]MeCN, 25 °C, TMS): $\delta =$ 10.03 – 10.0 (m, 24H), 9.93 (d, $J = 7.8$ Hz, 12H), 8.62 (d, $J = 8.1$ Hz, 24H), 8.48 (m, 18H), 8.43 (m, 6H), 8.27 (s, 24H), 8.23 (br d, 24H), 8.02 (d, $J =$ 4.2 Hz, 12H), 7.96 (m, 24H), 7.87 (m, 12H), 7.65 (dd, $J_1 = 12.7$ Hz, $J_2 =$ 5.6 Hz, 24H); UV/Vis (MeCN): $\lambda_{max}(\varepsilon) = 441$ (225 000), 370 (272 000), 303 (468 000), 280 (707 000), 264 (719 000); CD (MeCN): $\lambda_{min/max}(\Delta\varepsilon) = 464$ (76), 425 (−49), 270 (1756), 258 (−1261).

$[\Lambda_6\Lambda_3\Lambda_1$-**Ru$_{10}$**$][PF_6]_{20}$: ^{1}H NMR (500 MHz, [D$_3$]MeCN): $\delta = 10.03 - 10.0$ (m, 24H), 9.95 (d, $J = 7.5$ Hz, 12H), 8.63 (d, $J = 7.3$ Hz, 24H), 8.47 (m, 24H), 8.28 (s, 24H), 8.23 (d, $J = 8.3$ Hz, 24H), 8.04 (d, $J = 4.7$ Hz, 12H), 7.96 (m, 24H), 7.88 (dd, $J_1 = 8.1$ Hz, $J_2 = 5.6$ Hz, 12H), 7.66 (dd, $J_1 = 13.2$ Hz, $J_2 = 7.8$ Hz, 24H); UV/Vis (MeCN): $\lambda_{max}(\varepsilon) = 443$ (205 000), 371 (252 000), 303 (430 000), 279 (645 000), 264 (657 000); CD (MeCN): $\lambda_{min/max}(\Delta\varepsilon) = 477$ (178), 421 (−119), 272 (1639), 258 (−1220).

Positive electrospray – ionization mass spectra were obtained on a Jaguar time-of-flight mass spectrometer (Sensar Larson – Davis, Provo, UT). The electrospray interface was heated to 50 °C. The electrospray needle and the sampling cone potentials were 2100 V and 500 V, respectively. The samples were dissolved in MeCN ($1 - 5 \times 10^{-4}$ M). Sample solutions were introduced into the mass spectrometer with a microsyringe pump (PHD 2000 Harvard Apparatus, South Natick, MA) at a flow rate of 1.5 μL min^{-1} through PEEK tubing (64 μm i. d., Upchurch Scientific, Oak Harbor, MA). Resolution at *m*/*z* 800 was approximately 2700.

Electric birefringence measurements were obtained on a locally constructed instrument, described previously.[18] Computational modeling was carried out using the Spartan suite of programs (Wavefunction Inc., Irving, CA). Semiempirical calculations were performed on Silicon Graphics Indigo2 workstations using PM3(TM) method and parameters. The default optimization criteria for Spartan 5.0.3 were used in all cases. All optimized structures, including those of the tris-ruthenium(II) complexes of bipyridine, 1,10-phenanthrolene, and the $[(phen)_2Ru(tpphz)Ru(phen)_2]^{4+}$ dimer, lacked imaginary frequencies. The optimized PM3(TM) structures were then reoptimized by using molecular mechanics and Sybyl parameters. The computed bond lengths and angles in these complexes (both PM3(TM) and Sybyl-optimized structures) compared well with the bond lengths and angles reported from three-dimensional X-ray studies. The building blocks for the more complex structures were constructed by optimizing the $[Ru(phen)_2(tpphz)]^{2+}$ and the $[Ru(tpphz)_3]^{2+}$ complexes and then cleaving the resulting complexes at the dinitrogen bridges. These optimized building blocks were then assembled into the desired tetramers and decamers which were then optimized by using molecular mechanics and the Sybyl parameters. The three-dimensional space-filling molecular ion structures were generated by converting the optimized mechanics structures from Spartan to the UniChem (Ver. 4.1, Oxford Molecular, Oxford, UK) graphical user interface.

Received: May 26, 1999
Revised: September 3, 1999 [Z 13466]

[1] For recent reviews see: a) G. R. Newkome, E. He, C. N. Moorefield, *Chem. Rev.* **1999**, *99*, 1689; b) H.-F. Chow, T. K.-K. Mong, M. F. Nongrum, C.-W. Wan, *Tetrahedron* **1998**, *54*, 8543; c) D. A. Tomalia, R. Esfand, *Chem. Ind. London* **1997**, 416; d) F. Zheng, S. C. Zimmerman, *Chem. Rev.* **1997**, *97*, 1681.

[2] a) Z. Xu, M. Kahr, K. L. Walker, C. L. Wilkins, J. S. Moore, *J. Am. Chem. Soc.* **1994**, *116*, 4537; b) Z. Xu, J. S. Moore, *Angew. Chem.* **1993**, *105*, 1394; *Angew. Chem. Int. Ed. Engl.* **1993**, *32*, 1354.

[3] H. W. I. Peerlings, E. W. Meijer, *Chem. Eur. J.* **1997**, *3*, 1563.

[4] a) J. R. McElhanon, D. V. McGrath, *J. Am. Chem. Soc.* **1998**, *120*, 1647; b) P. Murer, D. Seebach, *Angew. Chem.* **1995**, *107*, 2297; *Angew. Chem. Int. Ed. Engl.* **1995**, *34*, 2116; c) D. Seebach, J.-M. Lapierre, K. Skobridis, G. Greiveldinger, *Angew. Chem.* **1994**, *106*, 457; *Angew. Chem. Int. Ed. Engl.* **1994**, *33*, 440; d) J. F. G. A. Jansen, H. W. I. Peerlings, E. M. M. de Brabander-Van den Berg, E. W. Meijer, *Angew. Chem.* **1995**, *107*, 1231; *Angew. Chem. Int. Ed. Engl.* **1995**, *34*, 1206; e) P. R. Ashton, S. E. Boyd, C. L. Brown, N. Jayaraman, S. A. Nepogodiev, J. F. Stoddart, *Chem. Eur. J.* **1996**, *2*, 1115.

[5] For recent reviews on this extensive field see: a) M. Fujita, *Chem. Soc. Rev.* **1998**, *27*, 417; b) J.-M. Lehn, *Supramolecular Chemistry, Concepts and Perspectives*, VCH, New York, **1995**.

[6] For a recent comprehensive review of this topic see: U. Knof, A. von Zelewsky, *Angew. Chem.* **1999**, *111*, 312; *Angew. Chem. Int. Ed.* **1999**, *38*, 303.

[7] a) V. Balzani, S. Campagna, G. Denti, A. Juris, S. Serroni, M. Venturi, *Acc. Chem. Res.* **1998**, *31*, 26; b) S. Campagna, G. Denti, S. Serroni, A. Juris, M. Venturi, V. Ricevuto, V. Balzani, *Chem. Eur. J.* **1995**, *1*, 211.

  0570-0833/00/3903-0618 $ 17.50+.50/0

[8] Recent reviews of stereospecific syntheses: a) F. M. MacDonnell, M.-J. Kim, S. Bodige, *Coord. Chem. Rev.* **1999**, *185–186*, 535; b) F. R. Keene, *Chem. Soc. Rev.* **1998**, *27*, 185; c) F. R. Keene, *Coord. Chem. Rev.* **1997**, *166*, 121.
[9] S. Bodige, A. S. Torres, D. J. Maloney, D. Tate, A. Walker, G. Kinsel, F. M. MacDonnell, *J. Am. Chem. Soc.* **1997**, *117*, 10364.
[10] A. S. Torres, D. J. Maloney, D. Tate, Y. Saad, F. M. MacDonnell, *Inorg. Chim. Acta*, in press.
[11] F. M. MacDonnell, M.-J. Kim, unpublished results.
[12] C. Moucheron, A. Kirsch-DeMesmaeker, A. Dupont-Gervais, E. Leize, A. Van Dorsselaer, *J. Am. Chem. Soc.* **1996**, *118*, 12834.
[13] D. J. Maloney, F. M. MacDonnell, *Acta Crystallogr. Sect. C* **1997**, *53*, 705.
[14] a) J. H. Brewster, *Top. Curr. Chem.* **1974**, *47*, 29; b) K. Mislow in *Topics in Stereochemistry*, *Vol 22* (Ed.: S. E. Denmark), Wiley, New York, **1999**, Chap. 1.
[15] S. Campagna, S. Serroni, S. Bodige, F. M. MacDonnell, *Inorg. Chem.* **1999**, *38*, 692.
[16] S. Campagna, A. Giannetto, S. Serroni, G. Denti, S. Trusso, F. Mallamace, N. Micali, *J. Am. Chem. Soc.* **1995**, *117*, 1754.
[17] S. Bodige, F. M. MacDonnell, *Tetrahedron Lett.* **1997**, *38*, 8159.
[18] N. Asgharian, X. Wu, R. L. Meline, B. Derecskei, H. Cheng, Z. A. Schelly, *J. Mol. Liq.* **1997**, *72*, 315.

On the Location of Li^+ Cations in the Fast Li-Cation Conductor $La_{0.5}Li_{0.5}TiO_3$ Perovskite**

José A. Alonso,* Jesús Sanz,* Jacobo Santamaría, Carlos León, Alejandro Várez, and Maria T. Fernández-Díaz

Interest in solids which conduct lithium ions has increased considerably in recent years because of the potential application of such solids in rechargeable lithium batteries. The ionic conductivity of $La_{2/3-s/3}Li_sTiO_3$ perovskites is one of the highest reported values in crystalline lithium cation conductors[1, 2] ($\sigma \approx 10^{-3}\ \Omega^{-1}cm^{-1}$ at $T = 300$ K), which makes these compounds good candidates for use as solid electrolytes in lithium batteries. The conductivities in the Pr and Nd perovskites are two and three orders of magnitude lower than for their La analogues.[2]

The perovskite structure (general formula ABO_3) can be regarded as a three-dimensional framework made up of vertex-sharing BO_6 octahedra with a large A cation in each of the 12-coordinated cavities of the framework. In the solid solution $La_{2/3-s/3}Li_sTiO_3$ ($0 \le s \le 0.5$) Li atoms were thought to replace La atoms at the A sites, which would lead to a progressive reduction of vacancies at these positions. However, the location of the Li atoms in the crystal structures of this family had not previously been possible from X-ray diffraction (XRD) data.

If the radius of the A cation is too small, the void is reduced in size by tilting of the BO_6 octahedra. The effect of tilting, when widely extended, is a predominant feature in the determination of the overall space-group symmetry of a particular perovskite. The precise structure determination of these oxides by XRD is particularly difficult because the superlattice reflections associated with the tilting of the TiO_6 octahedra arise from the oxygen atoms, which are weak scatterers when compared with La and Ti. Hence, neutron powder diffraction (NPD) measurements are more suitable for these investigations.

Following previous work,[3–5] we report a neutron powder diffraction study of the perovskite with the highest Li-substitution level, $La_{0.5}Li_{0.5}TiO_3$, in which we have, for the first time, located the Li^+ cations within the structure and have established the tilting scheme of the TiO_6 octahedra. Moreover, our data demonstrate that the solid solution mentioned does extend up to values of $s = 0.5$, a figure which had been controversial up to this time.

The powder sample of $La_{0.5}Li_{0.5}TiO_3$ exhibited excellent crystallinity, as shown by the sharpness of the XRD reflections (Figure 1a). The XRD pattern could be indexed in a cubic unit cell with $a = 3.8714(5)$ Å, characteristic of a perovskite structure. Nevertheless, the NPD pattern (Figure 1b) clearly showed the presence of superstructure reflections which could not be indexed in the simple cubic unit cell; these reflections arise from the tilting of the TiO_6 octahedra. Therefore, it was necessary to consider a larger unit cell. The reflections of the NPD diagram of $La_{0.5}Li_{0.5}TiO_3$ were indexed in an hexagonal unit cell with the systematic absences suggesting the space group $R\bar{3}c$ (no. 167). This rhombohedral space group corresponds to one of Glazer's octahedral tilt schemes for perovskite related structures,[6] which is adopted by a wide number of perovskites when the tilting angle of the octahedra remains small (for instance, $LaAlO_3$, $LaCuO_3$,or $LaNiO_3$).

A first Rietveld refinement was performed on a structural model in which Li atoms were not included; the starting parameters used were those of $LaNiO_3$[7] in the hexagonal setting of the space group $R\bar{3}c$ ($Z = 6$) with La placed at 6a (0,0,1/4), Ti at 6b (0,0,0), and oxygen at 18e (x,0,1/4) positions; the single x parameter was to be determined during the refinement. Unit cell parameters were $a = 5.4711(4)$, $c = 13.404(1)$ Å. The refinement of the La occupancy factor (over 6a positions) led to the expected value of 0.5 atoms per formula unit. This result seemed to exclude the possiblility that the Li cations are located at A sites of the perovskite, randomly distributed over the 6a positions together with La. This situation would have led to a significantly lower La occupancy factor, since the scattering length of Li is negative (see the Experimental Section). After the Rietveld refinement of this structural model, an R_{Bragg} factor of 0.074 was

[*] Dr. J. A. Alonso, Dr. J. Sanz
Inst. Ciencia de Materiales de Madrid
CSIC, Cantoblanco, 28049 Madrid (Spain)
Fax: (+349) 1-37-20-623
E-mail: ja.alonso@icmm.csic.es, jsanz@icmm.csic.es
Dr. J. Santamaría, Dr. C. León
F. C. Físicas, Univ. Compl. Madrid
28040 Madrid (Spain)
Dr. A. Várez
E.P.S., Univ. Carlos III
28911 Leganés (Spain)
Dr. M. T. Fernández-Díaz
Inst. Laue-Langevin, BP 156
38045 Grenoble Cedex 9 (France)

[**] This work was supported financially by Spanish CICyT (Spain, projects PB97-1181 and MAT98-1053-C04-03). The authors acknowledge ILL-Grenoble for making available time on the diffractometer.

  0570-0833/00/3903-0619 $ 17.50+.50/0